Atmos. Chem. Phys. Discuss., 15, 9661–9707, 2015
www.atmos-chem-phys-discuss.net/15/9661/2015/
doi:10.5194/acpd-15-9661-2015

Atmospheric Chemistry and Physics Discussions

New fire diurnal cycle characterizations to improve fire radiative energy assessments made from low-Earth orbit satellites sampling

N. Andela[1], **J. W. Kaiser**[2], **G. R. van der Werf**[1], **and M. J. Wooster**[3,4]

[1]Faculty of Earth and Life Sciences, VU University, Amsterdam, the Netherlands
[2]Max-Planck-Institut für Chemie, Mainz, Germany
[3]Kings College London, Environmental Monitoring and Modelling Research Group, Department of Geography, London WC2R 2LS, UK
[4]NERC National Centre for Earth Observation (NCEO), UK

Received: 2 January 2015 – Accepted: 10 March 2015 – Published: 31 March 2015

Correspondence to: N. Andela (n.andela@vu.nl)

Published by Copernicus Publications on behalf of the European Geosciences Union.

Abstract

Accurate near real time fire emissions estimates are required for air quality forecasts. To date, most approaches are based on satellite-derived estimates of fire radiative power (FRP), which can be converted to fire radiative energy (FRE) which is directly related to fire emissions. Uncertainties in these FRE estimations are often substantial. This is for a large part because the most often used low-Earth orbit satellite-based instruments like the MODerate-resolution Imaging Spectroradiometer (MODIS) have a relatively poor sampling of the usually pronounced fire diurnal cycle. In this paper we explore the spatial variation of this fire diurnal cycle and its drivers. Specifically, we assess how representing the fire diurnal cycle affects FRP and FRE estimations when using data collected at MODIS overpasses. Using data assimilation we explored three different methods to estimate hourly FRE, based on an incremental sophistication of parameterizing the fire diurnal cycle. We sampled data from the geostationary Meteosat Spinning Enhanced Visible and Infrared Imager (SEVIRI) at MODIS detection opportunities to drive the three approaches. The full SEVIRI time-series, providing full coverage of the diurnal cycle, were used to evaluate the results. Our study period comprised three years (2010–2012), and we focussed on Africa and the Mediterranean basin to avoid the use of potentially lower quality SEVIRI data obtained at very far off-nadir view angles. We found that the fire diurnal cycle varies substantially over the study region, and depends on both fuel and weather conditions. For example, more "intense" fires characterized by a fire diurnal cycle with high peak fire activity, long duration over the day, and with nighttime fire activity are most common in areas of large fire size (i.e., large burned area per fire event). These areas are most prevalent in relatively arid regions. Ignoring the fire diurnal cycle as done currently in some approaches caused structural errors, while generally overestimating FRE. Including information on the climatology of the fire diurnal cycle provided the most promising avenue to improve FRE estimations. This approach also improved the performance on relatively high spatiotemporal resolutions, although only when aggregating model results to coarser spatial and/or temporal

ACPD
15, 9661–9707, 2015

scale good correlation was found with the full SEVIRI hourly reference dataset. In general model performance was best in areas of frequent fire and low errors of omission. We recommend the use of regionally varying fire diurnal cycle information within the Global Fire Assimilation System (GFAS) used in the Copernicus Atmosphere Monitoring Services, which will improve FRE estimates and may allow for further reconciliation of biomass burning emission estimates from different inventories.

1 Introduction

Landscape fires are a global phenomena, and the annually burned area is roughly equivalent to the area of India (Giglio et al., 2013). Most burned area occurs in the savannas of Africa, Australia, and South America, where they shape ecosystem dynamics and due to their scale are an important source of global emissions of (greenhouse) gases and aerosols (Seiler and Crutzen, 1980; Bowman et al., 2009). Fires affect air quality both locally and regionally (Langmann et al., 2009), with recent studies putting mortality rates over 300 000 annually due to exposure to smoke (Johnston et al., 2012).

Traditionally, the amount of dry matter burned and quantity of trace gases and aerosols emitted have been calculated using biome-specific fire return intervals and estimates of the total amount of biomass as well as the fraction of biomass burned, the combustion completeness (Seiler and Crutzen, 1980). Thanks to new satellite input streams that better capture the spatial and temporal diffuse nature of fires, the estimated fire return intervals have been replaced by direct estimates of monthly, weekly or even daily area burned (Roy et al., 2005; Giglio et al., 2009). In addition, satellite information and biogeochemical modelling have been used to improve estimates of biomass and combustion completeness. However, uncertainties in these bottom-up fire emission estimates are still substantial (Reid et al., 2009; Zhang et al., 2012; Larkin et al., 2014), and they are generally inappropriate for use in near real-time systems partly because the burned area signature is only becoming detectable days to weeks after the actual fire occurrence.

ACPD
15, 9661–9707, 2015

Hot spot observations from satellite have been used as a proxy for burned area and emissions fluxes in near real time (Freitas et al., 2005; Reid et al., 2009; Wiedinmyer et al., 2011). Another promising and relatively new bottom up approach uses estimates of fire radiative power (FRP) observed from satellite to calculate daily fire radiative energy (FRE). Wooster et al. (2005) found that these FRE estimates scale directly to dry matter burned, potentially circumventing the uncertainties associated with estimating area burned, fuel loads, and the combustion completeness. In addition, FRP observations can be observed and processed in near real time (Xu et al., 2010; Kaiser et al., 2012; Zhang et al., 2012) and can be measured for small fires that remain undetected in burned area products (Roberts et al., 2011; Randerson et al., 2012).

Hot spot and FRP observations are currently the only available options when modelling exercises require near real time observations, for example in chemical weather forecasts used to predict air quality. The Global Fire Assimilation System (GFAS; Kaiser et al., 2012), for example, is used to estimate global near real time daily fire emissions within the EU-funded project Monitoring Atmospheric Composition and Climate III (MACC-III). GFAS is currently using fire observations from the polar orbiting MODerate-resolution Imaging Spectroradiometer (MODIS) instruments aboard the Terra and Aqua satellites (Giglio et al., 2006). Due to their relative proximity to the earth, the Terra and Aqua MODIS instruments have a high sensitivity to even quite low FRP (smaller and/or lower intensity) fires. However, they only provide four daily observations under ideal conditions but less when optically thick clouds are present, which may not be enough to fully characterize how fire activity varies over the course of the day. Observations with a much higher temporal resolution are available from geostationary satellites. However, as a consequence of their geostationary position, these satellites individually do not provide global data and are located at greater distance from the Earth resulting in typically coarser pixel sizes than polar orbiting instruments. Since the threshold of detectability of a fire is not only dependent on the instrument but also a function of the pixel area, geostationary sensors have a higher minimum FRP detection limit (typ-

ACPD
15, 9661–9707, 2015

ically > 40 MW) than MODIS (~ 8 MW). They therefore do not observe the lowest FRP component of the fire regime (Roberts et al., 2005; Freeborn et al., 2014).

Previous studies found that fire activity shows a strong diurnal cycle, and one that is both temporally and spatially variable (Prins and Menzel, 1992; Giglio, 2007; Roberts et al., 2009). The ideal set-up to detect fires would be a high temporal resolution imaging system, sensitive to even the lowest FRP fires, and providing global coverage, but due to the limitations of the orbital characteristics outlined above there is no single platform available to provide this. Therefore the measurement of FRE at a global scale is difficult, with polar orbiting satellites lacking observations to accurately represent the fire diurnal cycle and geostationary satellites being limited to certain regions of the globe and omitting the (rather common) low FRP fires. However, previous studies have developed approaches to estimate FRE based on the combination of data from different satellite systems (Boschetti and Roy, 2009; Ellicott et al., 2009; Freeborn et al., 2009, 2011; Vermote et al., 2009).

Some of these mixed approaches used both burned area and active fire data (Boschetti and Roy, 2009; Roberts et al., 2011), which may provide benefits in terms of more accurate FRE determination but cannot be used easily in near real time systems because of the latency in burned area observations. Alternatively, FRP observations of polar orbiting and geostationary satellites can be blended to combine the sensitivity of the MODIS instruments to lower FRP fires and the diurnal sampling characteristics of SEVIRI. Freeborn et al. (2009) developed a database for matching SEVIRI and MODIS FRP observations based on frequency-magnitude statistics, but the samples had to be accumulated over significant spatial areas (5°) to provide matchable statistics, which is incompatible with the need to develop a method operating at high spatial resolution. Freeborn et al. (2011) later presented an alternative approach, estimating FRE using MODIS data accumulated over 8 day periods over which MODIS samples a location at the fullest range of view zenith angles. The relationship between the "true" FRE and the limited number of FRP samples provided by MODIS was derived using SEVIRI FRP time-series sampled at the MODIS sampling interval. Vermote et al. (2009) and Ellicot

ACPD
15, 9661–9707, 2015

et al. (2009) used a different approach to create FRE data from MODIS, showing that for several regions of the globe the fire diurnal cycle can be described by a Gaussian distribution, and using monthly MODIS data to fit the parameters of the Gaussian. Using this approach, a first global estimation of monthly FRE was made (Ellicott et al., 2009). Despite the success of these latter approaches with regard to estimating FRE from MODIS, they are not a solution to the problem posed herein because they require 8 days of consecutive MODIS data and therefore cannot be applied in a near real-time approach.

Global fire emissions estimates at high spatial and temporal resolutions, ideally produced in near real time, are required to feed into atmospheric models which are under continuous development and run at improved resolutions thanks to increased computational power (Zhang et al., 2012). Higher temporal resolution may also help to reconcile bottom up and top down emission estimates (Mu et al., 2011). None of the approaches mentioned above are, however, suitable for providing this. Due to these limitations current state of the art global near real time emission inventories still ignore possible effects of fire diurnal cycle on their emission estimates (e.g., Wiedinmyer et al., 2011; Kaiser et al., 2012) and may therefore be structurally biased due to the fire diurnal cycle and the MODIS sampling design (e.g., Ichoku et al., 2008; Ellicott et al., 2009; Freeborn et al., 2011).

The purpose of the work presented here is to better understand the fire diurnal cycle and its spatiotemporal dynamics, in order to develop new ways to include this into a near real time fire emissions estimation framework. First, the spatial distribution and dependencies of the fire diurnal cycle and their effect on active fire detections at MODIS overpasses were explored. Then, data assimilation was used to develop three different methods to derive hourly FRE estimates at 0.1° resolution based on low Earth-orbiting observations, incorporating increasing knowledge about the fire diurnal cycle. Following previous studies (Freeborn et al., 2009, 2011), we used FRP observations derived from data collected by the geostationary SEVIRI instrument at MODIS detection opportunities, rather than actual MODIS observations, to drive the models and we evaluated

ACPD
15, 9661–9707, 2015

the model results against the full SEVIRI time-series. We used three years of active fire data (2010–2012) across Africa and the Mediterranean basin to include a wide range of climates and land cover types, and avoid the use of SEVIRI observations obtained at very far off-nadir angles over South America and northern Europe (Freeborn et al., 2014). Results are intended for application in GFAS within EU's Copernicus Atmosphere Monitoring Service (CAMS, http://atmosphere.copernicus.eu).

2 Data

To explore the spatiotemporal dynamics of the fire diurnal cycle, we used hourly temporal resolution FRP data derived from 15 min observations made by the SEVIRI instrument hosted onboard the geostationary Meteosat satellite (Sect. 2.1). However, to drive the models developed here we only used SEVIRI FRP observations made at the overpass times of the MODIS polar orbiting sensors (Sect. 2.2), whilst the hourly temporal resolution SEVIRI time-series were used to evaluate the results. Land cover characteristics (Sect. 2.3), along with data on fire size (Sect. 2.4), were used to better understand the spatial distribution of fire diurnal cycle. These datasets are described in more detail below, followed by the methods used in Sect. 3.

2.1 SEVIRI fire radiative power (FRP)

The SEVIRI instrument aboard the geostationary Meteosat Second Generation (MSG) series of satellites provides coverage of the full Earth disk every 15 min in 12 spectral bands (Schmetz et al., 2002). The Meteosat SEVIRI FRP-PIXEL product (Wooster et al., 2015) contains per-pixel fire radiative power data produced from the full spatial and temporal resolution SEVIRI observations. The FRP-PIXEL product is produced using an operational version of the geostationary Fire Thermal Anomaly (FTA) algorithm described in Roberts and Wooster (2008), and the product and its performance characteristics are described in Wooster et al. (2015). The FRP-PIXEL products are

ACPD
15, 9661–9707, 2015

freely available from the Land Surface Analysis Satellite Applications Facility (LSA SAF; http://landsaf.meteo.pt), from the EUMETSAT EO Portal (https://eoportal.eumetsat.int/) or via the EUMETCAST dissemination service (http://www.eumetsat.int) in both real-time and archived form, as detailed in Wooster et al. (2015). The Meteosat satellites are located at 0° longitude and latitude, and at nadir the SEVIRI pixels cover 3 km × 3 km on the ground, but this degrades with increasing view angle away from the West African sub-satellite point (Freeborn et al., 2011). The FRP-PIXEL product data used here were obtained from the LSA SAF and were rescaled to an hourly 0.1° resolution with the GFAS gridding algorithm explained in Kaiser et al. (2012). They were then archived (fsg3) in the Meteorological Archival and Retrieval System (MARS) of the European Centre for Medium range Weather Forecasting (ECMWF) prior to their use herein. Missing FRP values in individual observations within the hour (e.g., due to smoke or short periods of cloud cover) were thus implicitly ignored.

2.2 MODIS detection opportunity

The two MODIS sensors on board of the Terra and Aqua satellites provide 4 daily overpasses in most Earth locations, albeit sometimes at view angles in excess of 45° where the product performance is somewhat degraded (Freeborn et al., 2011). At nadir the MODIS thermal channel spatial resolution is 1 km, but decreases away from the swath centre (Freeborn et al., 2011). We used the MODIS MOD03 (Terra) and MYD03 (Aqua) geolocation products to determine where and when MODIS data were collected within the SEVIRI Earth disk. Because cloud cover may further limit the fire detection opportunity, we used the data quality and cloud cover information of the MOD14 and MYD14 active fire products to filter out grid cells with cloud cover (Giglio et al., 2006). Here we define the detection opportunity as the ability to make unobstructed observations, and the MODIS detection opportunity was derived by combining the MOD03, MYD03, MOD14 and MYD14 products, combining overpass times and cloud cover. We used MODIS data from Collection 5. Like the SEVIRI data, these data were rescaled to hourly 0.1° resolution with the GFAS gridding algorithm and archived

ACPD
15, 9661–9707, 2015

in MARS (Kaiser et al., 2012). The data were archived for the Terra (fs9s) and Aqua (fs9t) satellites separately. The original MODIS swath data can be downloaded from NASA at http://reverb.echo.nasa.gov.

2.3 MODIS Land cover

The dominant land cover type was derived from the MODIS MCD12C1 land cover product, which provides 0.05° spatial resolution annual information on land cover (Friedl et al., 2002). We calculated the dominant land cover type for each grid cell as the land cover type that on average covered the largest fraction during the study period (2010–2012). The University of Maryland (UMD) classification scheme was used, and data was rescaled to 0.1° resolution. Because we only considered Africa and the Mediterranean basin in this study, and because in some land cover classes very few fires occurred, we could merge some land cover classes that were of relatively little importance for our study. Specifically, all forest classes within the tropics were binned into the tropical forest class, while extratropical forests were all labelled temperate forest. Open and closed shrublands were merged into one shrubland class, and urban and built-up, barren or sparsely vegetated into grasslands.

2.4 Fire size

Here we define the fire size for a certain grid cell as the mean burned area per fire event, weighted by their total area burnt (when calculating the mean, a fire event burning 100 km^2 is assigned one hundred times the weight of an event burning 1 km^2). The MODIS MCD64A1 burned area product provides daily mapped estimates of global burned area (Giglio et al., 2009). We applied the methods described by Archibald and Roy (2009) to derive a global mean fire "size" (area) map using 2001–2013 data. We made one modification to the approach described by Archibald and Roy (2009): we assumed that two neighbouring burned area grid cells only belonged to the same fire if the burn date was no longer than two days apart (instead of 8 days). We believe

ACPD
15, 9661–9707, 2015

that overall this provides a better estimation of the fire size in our study region, as the vast majority of fires here are grass fires, occurring outside tropical forest zones and thus spreading relatively fast while being relatively less often obstructed by cloud cover. Consequently, the uncertainty in burn date is generally low in our study region (Giglio et al., 2013) and so the two day thresholds was deemed more appropriate.

3 Methods

Our overall goal within GFAS is to provide hourly estimates of FRE at 0.1° spatial resolution, based on the limited number of MODIS overpasses available each day at each grid cell location. This limited number of daily MODIS observations, in combination with the often pronounced fire diurnal cycle, are the major obstacles in providing the required output. We first studied the spatiotemporal variation of the fire diurnal cycle, in an attempt to understand its variability (Sect. 3.1). Then, we explored the way the fire diurnal cycle affects active fire detections made at the MODIS sampling times (Sect. 3.2). Using this knowledge we explored three independent methods to parameterize the fire diurnal cycle. Building on the work of Freeborn et al. (2009, 2011), to drive the three modelling approaches we used SEVIRI data sampled at the MODIS detection opportunities (according to the hourly data representation introduced above), rather than actual MODIS observations (Sect. 3.2). This allowed us to focus on the issue of diurnal cycle sampling rather than simultaneously dealing with the issue of MODIS and SEVIRI's differential sensitivity to active fires (Freeborn et al., 2009).

Using data assimilation we combined the discrete actual SEVIRI observations, made at the time of the MODIS detection opportunities, with hourly predictions of fire activity – using their combination to create continuous hourly best estimate FRE time-series (Sect. 3.3). We developed three prediction methods, each based on increasingly detailed knowledge of the fire diurnal cycle. The first method was the most parsimonious and assumed persistent fire activity until the next satellite detection opportunity (Sect. 3.4). The second method followed previous studies and used a Gaussian func-

ACPD
15, 9661–9707, 2015

tion to predict fire development over the day (Vermote et al., 2009; Sect. 3.5). The third method combined a Gaussian function to describe the fire diurnal cycle with prior knowledge about the climatology of the fire diurnal cycle per land cover, to better estimate the parameters of the Gaussian function (Sect. 3.6). Comparing the results of the three approaches to those from the full hourly SEVIRI time-series allowed us to determine and discuss their strengths and limitations (Sect. 3.7).

3.1 Exploring the fire diurnal cycle

We started exploring the fire diurnal cycle and its drivers. A Gaussian function was optimally fitted (least squares) to the hourly SEVIRI observations $\widetilde{\rho}_{\mathrm{SEV}(t)}$ for each grid cell and day of fire activity during the study period:

$$\widetilde{\rho}_{\mathrm{SEV}(t)} = \rho_{\mathrm{base}} + \left(\rho_{\mathrm{peak}} - \rho_{\mathrm{base}}\right) \mathrm{e}^{-\frac{\left(h_t - h_{\mathrm{peak}}\right)^2}{2\sigma^2}}. \quad (1)$$

Where ρ_{base} corresponds to the nighttime fire activity, ρ_{peak} to the maximum FRP for a given day, σ is the SD of FRE distribution over the day (dependent on fire duration), h_t is the local solar time at time step t and h_{peak} is the local hour at which FRP reaches its daily maximum. This resulted in a database containing hourly time-series of $\widetilde{\rho}_{\mathrm{SEV}(t)}$ and the fitted Gaussian function, and daily time-series of optimal parameter values of the Gaussian function for each grid cell. At the same time we also kept track of hourly MODIS detection opportunities. This enabled us get a better understanding of structural errors caused by the MODIS sampling design in relation to the actual fire diurnal cycle.

Although the fire diurnal cycle as observed by SEVIRI is comparable to that which would be observed by MODIS if it had the same temporal sampling ability, it is a little different due to SEVIRI's inability to discriminate the lowest FRP fire pixels which typically dominate more towards the start and end of the daily fire cycle, but which are also present along with often higher FRP pixels towards the diurnal cycle maxima (Freeborn et al., 2009). To gauge the magnitude of the effect Freeborn et al. (2009) derived the

ACPD
15, 9661–9707, 2015

"virtual MODIS" fire product that has the temporal sampling of SEVIRI and the sensitivity to fire of MODIS. They found that the full-width at half maximum height (i.e., the width of the diurnal cycle at half of the daily FRP maximum value) of the diurnal cycles derived from the SEVIRI and the "virtual MODIS" datasets are very similar, it is the amplitude and the full-width at base height of the two cycles, which are more different. In terms of total FRE emitted, the latter is of less importance, here we followed Freeborn et al. (2011) in assuming that the diurnal cycles from SEVIRI and MODIS are sufficiently similar.

In order to visualize the spatial distribution of fire diurnal cycle, the climatological diurnal cycle was calculated for each grid cell depending on the mean parameter values of the Gaussian function weighted for daily FRE, including all days of fire activity during the study period without cloud obscurance. To get a better understanding of the drivers of the fire diurnal cycle these results were compared to land cover and aspects of the fire regime (fire size, total annual FRE, and the annual number of days with fire activity), see Sect. 2.

3.2 Sampling SEVIRI data at MODIS detection opportunities

During the data assimilation, SEVIRI observations at MODIS detection opportunities were used to drive the models. Here, SEVIRI observations for a given hour t are given by $\widetilde{\rho}_{\mathrm{SEV}(t)}$ and SEVIRI fraction of observed area by $\widetilde{\alpha}_{\mathrm{SEV}(t)}$; in the same way, observations of the MODIS instruments are given by $\widetilde{\rho}_{\mathrm{MOD}(t)}$ and $\widetilde{\alpha}_{\mathrm{MOD}(t)}$. Therefore input for the models, i.e., the SEVIRI observations at MODIS detection opportunity times ($\widetilde{\rho}_t$ and $\widetilde{\alpha}_t$) for a given hour t are given by:

$$\widetilde{\rho}_t = \widetilde{\rho}_{\mathrm{SEV}(t)} \quad (2)$$

$$\widetilde{\alpha}_t = \widetilde{\alpha}_{\mathrm{MOD}(t)}. \quad (3)$$

For clarity, we assumed that the observed FRP $\widetilde{\rho}_t$ is zero when there was no MODIS detection opportunity. Anyhow, during the data assimilation $\widetilde{\rho}_t$ was weighted for observed area $\widetilde{\alpha}_t$, which was zero when there was no observation.

ACPD
15, 9661–9707, 2015

SEVIRI data sampled at MODIS detection opportunities were compared to the full SEVIRI hourly time-series to explore the effect of the fire diurnal cycle on the daily sampling at MODIS overpasses. More specifically we calculated the percentage of FRE emitted on days without any active fire detection at MODIS detection opportunities, and the total daily number of MODIS overpasses during the fire season. The latter was calculated by weighing the mean number of monthly detection opportunities at MODIS overpasses by monthly total detected FRP, thus giving the largest weight to the month with most fire activity (ignoring cloud cover).

3.3 Data assimilation

We used a modified version the fire data assimilation methodology of GFAS to allow representation of the diurnal cycle. GFAS assumes that the availability of observations dominates the error budget of the global FRP fields. It approximates these errors by further assuming the FRP variance to be inversely proportional to the fraction of observed area $\widetilde{\alpha}_t$. Thus the variance increases with decreasing partial cloud cover and with the number of satellite observations. In the following data assimilation, GFAS fills observation gaps with a Kalman filter, in which current observations are combined with information from earlier ones. The Kalman filter has a time step of 1 day. It uses a trivial predictive model for the temporal evolution of FRP, i.e., persistence, and assumes for the accuracy of the 1 day FRP prediction that the variance increases by a factor of 9 (Kaiser et al., 2012).

Our modifications affected the step size and the FRP prediction model. The former was set to 1 h to be able to represent a diurnal cycle. For calculating the FRP prediction ρ_t, we investigated three different approaches, cf. Sects. 3.4–3.6 below. They included increasing a priori knowledge about the diurnal cycle. In all three cases, we assumed for the accuracy of the 1 h FRP prediction that the variance increases by a factor of 4. Lowering the value compared to the daily GFAS is motivated by the shorter time step used in our study. However, lowering it too much would not give sufficient weight to new FRP observations. Thus the analysis FRP $\hat{\rho}_t$ and "fraction of observed area" $\hat{\alpha}_t$ were

ACPD
15, 9661–9707, 2015

calculated at each 1 h time step by optimal interpolation as follows, cf. Eqs. (32)–(33) of Kaiser et al. (2012):

$$\hat{\rho}_t = \frac{1}{\hat{\alpha}_t}\left(\frac{\hat{\alpha}_{t-1}}{5}\rho_t + \tilde{\alpha}_t\tilde{\rho}_t\right) \tag{4}$$

with ρ_t according to Sects. 3.4–3.6 and

$$\hat{\alpha}_t = \frac{\hat{\alpha}_{t-1}}{5} + \tilde{\alpha}_t. \tag{5}$$

3.4 Persistent approach

Applying the daily persistence approach of Kaiser et al. (2012) to hourly time resolution, we first explored the most parsimonious approach that predicts FRP ρ_t as being equal to the FRP of the previous time step's analysis:

$$\rho_t = \hat{\rho}_{t-1}. \tag{6}$$

This approach provided insights in the spatiotemporal consequences for FRE estimation when information on the fire diurnal cycle is not incorporated.

3.5 Dynamic approach

In the second approach we assumed no prior knowledge about the fire diurnal cycle, but followed previous studies of Vermote et al. (2009) and Ellicot et al. (2009) and the recommendation in Kaiser et al. (2009) to use a Gaussian function to describe a "standard fire diurnal cycle". The prediction was calculated by optimally fitting a Gaussian function through the last 24 h of analysis:

$$\rho_t = \rho_{\text{base}} + \left(\rho_{\text{peak}} - \rho_{\text{base}}\right) e^{-\frac{\left(h_t - h_{\text{peak}}\right)^2}{2\sigma^2}} \tag{7}$$

ACPD
15, 9661–9707, 2015

with ρ_{base}, ρ_{peak}, h_{peak} and σ derived from fitting ρ_t to

$$\hat{\rho}_{t-24}, \hat{\rho}_{t-23}, \ldots, \hat{\rho}_{t-1}. \quad (8)$$

In contrast to the climatological approach described below, all parameters of the Gaussian function (ρ_{base}, ρ_{peak}, σ and h_{peak}) were derived by minimizing the sum of least squares between the Gaussian function and the previous 24 h of the analysis. Finally, if during the last 24 h no active fires were detected at the MODIS overpass times, the prediction was assumed to be zero.

3.6 Climatological approach

The third approach followed the dynamic approach by optimally fitting a Gaussian function through the last 24 h of the analysis (Eqs. 7 and 8). However, now only h_{peak} was optimally fitted. Following previous studies that found that fire diurnal cycle is land cover dependent (Giglio, 2007; Roberts et al., 2009; Vermote et al., 2009; Freeborn et al., 2011), we used land cover (LC) average values σ_{LC} for σ (weighted by FRE). Values of ρ_{base} and ρ_{peak} on the other hand could be directly related to daily MODIS observations. We followed Vermote et al. (2009) to use the mean of the nighttime (defined here as 6 p.m.–6 a.m. the next day) observations at MODIS detection opportunities to determine ρ_{base}. To relate SEVIRI observations at MODIS detection opportunities to ρ_{peak} the ratio of mean daytime (6 a.m.–6 p.m.) FRP observations at MODIS detection opportunities to mean ρ_{peak} was calculated per land cover type. We used per land cover average values for scaling the daytime observations at MODIS detection opportunities to ρ_{peak} rather than the values found per grid cell to keep the model generic and globally applicable. Finally, if there were no active fires observed during the previous 24 h, we forced the prediction to be zero, to prevent fires from continuing during long periods of no observations.

ACPD
15, 9661–9707, 2015

3.7 Model evaluation

Finally, the best estimated hourly FRE fields (or analysis; $\hat{\rho}_t$) resulting from the three different modelling approaches (persistent, dynamic and climatological) were evaluated via comparison to those derived from the hourly SEVIRI time-series (see Sect. 2.2). We used two criteria to evaluate the model performance: first, the spatial distribution of FRE estimates; and second, the temporal distribution of FRE. The spatial performance of the three modelling approaches was assessed via their ability to reproduce the annual mean FRE per land cover type, and by comparing the spatial distribution of FRE as estimated by the modelling approaches and as derived from SEVIRI over the study region and period. The temporal performance was assessed via the ability of the model to allocate the emitted energy in the right grid cell at the right moment in time, for which we used Pearson's r between the three modelling approaches and the SEVIRI data at four different spatiotemporal resolutions (0.1° and 1° spatial, and hourly and daily temporal resolution). When calculating Pearson's r between the hourly model results and SEVIRI data we included cloud free days only, while the daily model results were compared to the full cloud cover corrected SEVIRI times series, using a simple cloud cover correction method explained below. We appreciate that for specific instances, e.g., a study with a focus on individual fires, or large fires only, different criteria could be used, which we will further elaborate in the discussion. Wooster et al. (2005) and Roberts et al. (2009) already demonstrated that SEVIRI observations sample the diurnal cycle of large fires well, and for some individual large fires show FRP time-series that depict diurnal characteristics appearing close to Gaussian in nature even at 15 min temporal resolution.

Finally, we compared daily regional aggregated time-series for several study regions of the three modelling approaches and SEVIRI. In order to compare daily regional time-series to the model, a cloud cover correction needed to be carried out. Because persistent cloud cover is relatively rare during the burning season in most parts of Africa, we chose a simple gap filling approach where the value of the last cloud-free observation

ACPD
15, 9661–9707, 2015

is assumed to be valid until the next cloud-free observation, which is consistent with the observation gap filling in the daily GFAS.

4 Results

4.1 The diurnal cycle and MODIS sampling

First, we present the results related to the spatial distribution of the fire diurnal cycle, and assess the impact of the fire diurnal cycle on active fire observations made at the times of the MODIS overpass. The spatial distribution of the fire diurnal cycle was explored by optimally fitting a Gaussian function to the hourly, 0.1° SEVIRI FRP time-series. Reasonable overall correlations between SEVIRI and the optimally fitted Gaussian functions were found (Pearson's $r = 0.55$; weighted mean for all grid cells), while a Gaussian was better able to describe hourly fire activity in regions where fires could spread over large areas and were characterized by high ρ_{peak} (e.g., for fire size $< 10\,km^2$ $r = 0.51$, for 10–50 km^2 $r = 0.56$, and $> 50\,km^2$ $r = 0.63$). This is likely to be in part related to the fact that characterisation of the diurnal cycle of "smaller" fires will be more affected by instances of SEVIRI failing to detect one or more of their fire pixels than would larger fires, hence introducing more variability into the apparent diurnal cycle. Whilst the SEVIRI FRP-PIXEL product shows apparently the best performance metrics of any current geostationary fire product derived from SEVIRI data (Baldassarre et al., 2015), such failures in active fire pixel detection clearly occur, for example simply due to fire pixels being too low in their FRP to detect by SEVIRI, along with a variety of potential other factors (Wooster et al., 2015).

Figure 1 shows an example of two 0.1° grid cells in which the hourly average FRP maxima reached relatively high levels, well in excess of 1 GW, and fire persisted for several days. As with the individual fires, shown by SEVIRI in Wooster et al. (2005) and Roberts et al. (2009), the FRP from these fires appears to drop to zero, or near zero, every night. This is a consequence both of the actual FRP from the fire significantly

ACPD
15, 9661–9707, 2015

diminishing at this time due to, for example, fuel moisture, wind and other ambient atmospheric conditions being far less conducive to intense fire activity by night than by day (Hély et al., 2003; Gambiza et al., 2005), but also because some or all of these lower FRP fire pixels will have FRPs below the SEVIRI active fire pixel detection limit of around 40 MW (Roberts and Wooster, 2008). At the start of the following day, fuel moisture and ambient atmospheric conditions generally become more conducive to fire, and fire intensities and rates of spread typically increase once more such that more of the fire-affected pixels breach the SEVIRI FRP detection limit (Roberts et al., 2009).

The results shown in Fig. 1 indicate that high FRP, relatively long-lived fire activity is rather well described by a Gaussian function, even at this 0.1°, hourly resolution which is significantly higher than that used in previous studies fitting Gaussian descriptors to remotely sensed measures of active fire activity. At the same time, it also became apparent that observations from a MODIS-type sampling interval are not always representative of the daily fire activity. The inability of the MODIS sampling times to provide representative observations is well illustrated in Fig. 1a, where on the first day of the fire the morning and afternoon time of MODIS sampling slot almost completely missed the fire activity.

The shape of the Gaussian function, and consequently the parameters: SD (σ) peak fire activity (ρ_{peak}) and corresponding hour (h_{peak}), varied considerably over the individual days (Fig. 1). For example, in the African savanna grid cell (Fig. 1c), fire activity on day 3 continued longer in the afternoon compared to day 4, when conditions somehow became less favourable for maintaining the fire earlier in the afternoon. Therefore, the shape of the fire diurnal cycle was dependent on spatiotemporal scale. When diurnal fire activity was aggregated over several days, which can be compared to using a coarser temporal or spatial resolution, σ increased as compared to fire activity for individual days (compare Fig. 1a with b, and Fig. 1c with d). The relatively narrow diurnal cycle of the individual days have varying peak hours of fire activity, so that the sum of it is wider than any of the individual cycles and the peak fire activity less pronounced.

ACPD
15, 9661–9707, 2015

In addition to an observed variability in the fire diurnal cycle seen on different days, we found distinct spatial patterns in the optimal fitted Gaussian parameters (Fig. 2). Some of these patterns were similar for the different parameters. In particular, there were zones of generally more intense fires (e.g., South Sudan, northern Central African Republic, Botswana, Namibia and parts of Angola and the Democratic Republic of the Congo (DRC)), showing relatively high values of ρ_{peak}, ρ_{base} and σ compared to other zones where values for all three parameters were relatively low (e.g., Zambia, Mozambique, Tanzania, Nigeria and Cameroon). On top of this general pattern, a clear gradient is visible as you move from drier to more humid regions, seen most clearly when moving from Namibia via Angola to DRC. In more humid savannas, when fuel conditions were optimal, high ρ_{peak} values could be reached but fire duration over the day was generally short and night time FRP values were more likely to fall below the SEVIRI FRP detection threshold (Fig. 2). h_{peak} varied considerably over the study region, with areas showing most fire activity late in the afternoon generally in more humid or forested regions but also in some more arid regions (Fig. 2d).

Table 1 shows the land cover-averaged values of the results presented in Fig. 2. In addition we calculated the ratio of the mean SEVIRI FRP at MODIS daytime detection opportunities to the maximum daytime FRP ρ_{peak}. These results were used in the third modelling approach that combined the fire diurnal cycle climatology with observations made at the MODIS sampling times to derive the daily fire diurnal cycle predictions (see Sect. 3.6). More intense fires with long duration and high peak values were associated with fires in shrublands, savannas and grasslands, while a more pronounced fire diurnal cycle was present in more humid woody savannas or tropical forests. The ratio of mean daytime FRP made at the MODIS sampling times and ρ_{peak} was relatively constant for various land cover types with ρ_{peak} generally about three times as large as the mean FRP at the daytime MODIS detection opportunities (Table 1).

In order to better understand the spatial distribution of the fire diurnal cycle features, we studied characteristics of the fire regime that were expected to be related to fuel properties and the diurnal cycle (Fig. 3a, c and d). To guide the interpretation we have

ACPD
15, 9661–9707, 2015

included a land cover map, partly governing fuel loads, in Fig. 3b. Annual emitted FRE varied widely over the study region, and highest values were found in the savannas and woody savannas (compare Fig. 3a with b) and coincided with regions of large fire size and/or a high number of annual fire days (compare Fig. 3a with c and d). Similarities with characteristics of the fire diurnal cycle were also found, the earlier mentioned zones of generally more intense fires (high values of ρ_{peak}, ρ_{base} and σ) often coincided with regions of large fire size (Figs. 2a–c and 3c). In the more humid tropical areas, high ρ_{peak} values occurred in areas of relatively large fire size and/or a high number of annual fire days (Figs. 2a and 3c, d).

The relative fraction of FRE emitted on days that SEVIRI data sampled at MODIS observation times did not observe active fires is an important factor affecting model performance, and showed similar spatial patterns as σ, indicating that duration of fires over the day plays an important role (Figs. 2c and 4a). In addition, the geographical location and cloud cover during the burning season played a role by affecting the effective number of daily MODIS observations (Fig. 4b). The peak hour of fire activity also played a role, and especially in more humid areas with frequent cloud cover and late afternoon fire activity sometimes over 50 % of FRE was emitted on days without any SEVIRI active fire detections at MODIS detection opportunities (compare Figs. 2d and 4a). This clearly demonstrates the value of the data provided by the very high temporal resolution geostationary systems, even though they are unable to resolve and detect fire pixels as low in FRP as those from polar orbiters (Roberts and Wooster, 2008).

4.2 Model evaluation

To evaluate the three modelling approaches that estimated FRE from SEVIRI data only at the MODIS sampling times we started with comparing the spatial distribution of mean estimated FRE for each method with the cloud corrected SEVIRI FRE calculated using the entire hourly, 0.1° SEVIRI FRP dataset (see Sect. 3.7; Fig. 5). The three methods yielded very different results, with a general overestimation by the persistent approach, underestimation by the dynamic approach, and overall good performance of

ACPD
15, 9661–9707, 2015

the climatological approach when compared to the FRE calculated using the full SEVIRI dataset. However, whilst this reflects the general pattern, the performance bias was not homogeneous over the region. The persistent approach showed best results for regions with long daytime fire durations (i.e., large σ) and with a late peak in fire activity; the dynamic approach also did comparatively well in areas that were characterized by such long fire durations; and although performing generally better than the other methods, the climatological approach showed a general underestimation for areas of relatively late peak fire activity (compare Figs. 2 and 5). To a certain extent these regional differences correspond to the distribution of the different land cover types (Table 2). For example, for temperate forests and shrublands the persistent modelling approach showed notably better comparison to the FRE derived via the entire SEVIRI dataset, while the climatological modelling approach overestimated FRE.

Equally important as the absolute FRE intercomparisons shown in Fig. 5 and Table 2 are their temporal dynamics. Figure 6 shows regional daily budgets for several study regions with different geographical positions and land cover. Similar to the results in Fig. 5, we found a general overestimation by the persistent approach, underestimation by the dynamic approach, and best overall estimation by the climatological approach. Overestimation of the persistent approach was occurring mostly in the tropics (e.g., Nigeria and DRC), where also stronger day to day variability was observed as compared to that derived with the complete SEVIRI data or the other modelling approaches (Fig. 5b and c). Both the dynamical and climatological approaches showed a small delay in their FRE estimations compared to the complete SEVIRI dataset.

To further test the ability of the three modelling approaches to allocate FRE to the individual grid cells at the right moment in time, correlation coefficients were calculated. Table 3 shows Pearson's r between SEVIRI and the three modelling approaches at 0.1° spatial and daily temporal resolution including all days without cloud cover during the three year study period. A striking increase in correlation was observed when aggregating model results further to a 1° resolution. Freeborn et al. (2009, 2011) previously demonstrated the value of such spatial aggregation when deriving relationships

ACPD
15, 9661–9707, 2015

between SEVIRI and MODIS datasets, and this technique is currently used within the near real-time SEVIRI FRP-GRID products produced by the LSA SAF from the SEVIRI FRP-PIXEL data (Wooster et al., 2015). At 0.1° resolution the best correlations were found for shrublands and savannas while for aggregated data best performance was found for woody savannas and savannas. At 0.1° the persistent approach performed best while at 1° spatial resolution the persistent and climatological approaches did equally well.

When moving to hourly resolution, the model performed less well but a similar increase in the correlation coefficient was observed when increasing the spatial scale to 1° (Table 4). In contrast to the daily results, the dynamic and climatological approaches generally performed better than the persistent approach at hourly resolution.

5 Discussion

Unlike biomass burning emission inventories based on burned area, inventories using active fire observations from Earth Observation satellites can be produced in near real time (Freitas et al., 2005; Reid et al., 2009; Sofiev et al., 2009; Wiedinmyer et al., 2011; Kaiser et al., 2012; Darmenov and da Silva, 2013). The near real time emissions inventories are, at present, generally based on active fire data from the MODIS instruments operating onboard the Terra and Aqua polar orbiting satellites. The FRP observations of MODIS are almost without saturation, operating day and night, with a reasonable spatial resolution and with new observations available for any location at least a few times every day – cloud cover permitting. However, it is well known that fire activity in most regions follows a clear daily cycle (e.g., Roberts et al., 2009; Vermote et al., 2009). Consequently, the FRP measures derived from intermittent polar orbiting MODIS observations are often not fully and directly representative of the actually daily fire activity (Fig. 1; Giglio, 2007; Vermote et al., 2009; Freeborn et al., 2011). Although several approaches have been developed to obtain more accurate estimations of FRE from the limited temporal sampling of FRP provided by MODIS (e.g., Ellicott et al.,

ACPD
15, 9661–9707, 2015

2009; Freeborn et al., 2009, 2011; Vermote et al., 2009), they are all best suited to be used with previously collected and/or aggregated FRP data, and none can be readily implemented at high spatiotemporal resolution in near real time. For this reason, most current global emission inventories produced in near real time actually ignore fire diurnal dynamics completely (e.g., Kaiser et al., 2012), and this results in large biases in the FRE budgets (Ellicott et al., 2009; Zhang et al., 2012).

Here we start discussing the spatial distribution of the fire diurnal cycle, and its drivers (Sect. 5.1). Building on previous work, we developed and compared several methods to estimate hourly FRE in near real time from observations made by SEVIRI at MODIS detection opportunities. The new methods illustrate how MODIS observations might be used to calculate FRE, and where errors can be expected due to the diurnal cycle and the limited temporal sampling provided by MODIS (Sect. 5.2).

5.1 Exploring the fire diurnal cycle using a Gaussian function

The fire diurnal cycle characteristics were explored by fitting of a Gaussian function to the hourly SEVIRI time-series. Vermote et al. (2009) and Ellicott et al. (2009) found that at a 0.5° monthly resolution the fire diurnal cycle can be described by a Gaussian function, using MODIS observations to resolve the unknown parameters. They choose the spatiotemporal size of the study regions such that a statistical representative number of fires and MODIS FRP detections were included, and the observations covered the full range of MODIS view angles – since the sensitivity of MODIS to fire depends upon this (Vermote et al., 2009). Although later work showed that in fact fire activity may be somewhat skewed in the afternoon, here we found that even at a high spatiotemporal resolution (0.1°; hourly) a Gaussian function provides a fairly robust description of the fire diurnal cycle. However, at 0.1° hourly resolution, SEVIRI data sampled at the MODIS detection opportunities does not always provide enough information to adequately depict fire activity for an individual grid cell and day (Fig. 1). Moreover, the spatiotemporal scale at which we observe the fire diurnal cycle has a significant impact on its shape. When moving to a coarser spatiotemporal resolution, the shape of the

ACPD
15, 9661–9707, 2015

diurnal cycle likely becomes wider, with less pronounced peaks. This is mostly a consequence of the spatiotemporal variation in hour of peak fire activity of the individual fires or fire days (Fig. 1). Therefore, typical values of the parameters of the Gaussian found in this study (Fig. 2) do not necessarily correspond to typical values found by earlier studies (e.g., Roberts et al., 2009; Vermote et al., 2009), who used much larger sample sizes (i.e., spatiotemporal resolutions). Likewise the results presented here are not necessarily representative for individual fires.

Although the shape of the "average" fire diurnal cycle is scale dependent, regional patterns in the diurnal cycle characteristics (Fig. 2) remain similar over different scales, and therefore we found similar land cover dependent characteristics as previous studies. For example, shrublands and grasslands generally faced drier conditions when burning than did woody savannas or tropical forest, and therefore fire activity typically continued longer over the day and the hour of peak fire activity was generally located later in the afternoon (Fig. 2; Table 1; Giglio, 2007; Roberts et al., 2009). For the same reason, temperate and boreal forests have been reported to show a more pronounced diurnal cycle than grasslands (Fig. 2; Sofiev et al., 2013; Konovalov et al., 2014). Building on the land cover based analysis of Roberts et al. (2009), we provide a first analysis of the spatial distribution of the fire diurnal cycle.

The three parameters determining the shape of the Gaussian can be used to visualize the spatial distribution of the fire diurnal cycle. The daily FRP-maximum is given by ρ_{peak}, fire duration over the day by σ, and the baseline FRP by ρ_{base}. Similar spatial patterns were found for all three parameters mentioned above (Fig. 2a, b and c). This indicates that there are zones of generally more "intense" fires with high ρ_{peak}, large σ and higher ρ_{base}, while other zones are characterised by lower intensity fires. In land cover classes where most of the fires were grass fuelled (grasslands, savannas and woody savannas), a considerable part of the spatial variation in fire diurnal cycle could be explained by fire size (see Sect. 2.4; Figs. 2 and 3). Large fires were often found in frequently burnt and/or more arid areas (Fig. 3a) where high fuel connectivity, low fuel density and low fuel moisture allow relatively fast moving fires with large fire fronts to

ACPD
15, 9661–9707, 2015

form (Hély et al., 2003; Sow et al., 2013). Besides fire size and land cover, part of the variability in the fire diurnal cycle could be explained by a gradient in diurnal weather conditions. Grass fuelled large fires were also common in the more humid savannas of southern Africa, but here nighttime weather conditions appear to become rather unfavourable for fire (Figs. 2b and 3c). In humid savannas ρ_{peak} values were not solely associated with large fire size, but also with areas showing a high number of annual days with fire activity and may be explained by several relatively small fires burning at the time. The high number of fire days may indicate a larger number of fire ignitions and/or that fires are spreading at a slower rate due to the more pronounced fire diurnal cycle, higher humidity, or higher fuel density (Hély et al., 2003; Sow et al., 2013). Finally, in the Mediterranean basin the relatively low fire return period, and consequently higher fuel density, may also cause relative intense fires with long duration over the day (Fig. 2; Archibald et al., 2013).

The peak hour of fire activity found here corresponds to the moment of day at which 50 % of the total FRE has been emitted (assuming $\rho_{base} \ll \rho_{peak}$), and it did not always correspond to the peak hour of fire activity found by previous studies (Fig. 2d; e.g., Giglio, 2007; Roberts et al., 2009; Vermote et al., 2009). In general most FRE was emitted during the afternoon, and clear spatial patterns were present in the typical peak hour of the Gaussian. High values of h_{peak} were found in regions of higher fuel density or in more arid areas where fires could spread over large areas (Figs. 2d and 3). In arid regions with large typical fire sizes, fire spread was often fast and a 0.1° grid cell only corresponded to a part of the actual fire resulting in large variation in h_{peak} between neighbouring grid cells (Fig. 2d).

5.2 Model performance and the MODIS sampling design

Data assimilation and three different modelling approaches, depending on increasing knowledge of the fire diurnal cycle, were used to estimate hourly FRE from SEVIRI FRP data sampled at the times of MODIS detection opportunities. Here we start discussing the performance of the different methods with respect to daily and regional FRE es-

ACPD
15, 9661–9707, 2015

timations. Then we discuss the more uncertain model performance for individual grid cells at an hourly resolution.

The persistent approach is comparable to a direct hourly extension of the current GFAS methods (Kaiser et al., 2012), where the fire diurnal cycle is ignored and the predicted FRP for each hour is equal to that of the last FRP observation. This led to a general overestimation of daily FRE because the 13:30 LT temporal sampling time of MODIS is relatively close to the peak hour of daily fire activity, and therefore not very representative of the full period until the next observation at 22:30 LT (Figs. 2d and 5; Table 2). Moving away from the equator, the number of daily MODIS observations increases due to orbital convergence at higher latitudes, and consequently the model performance improved (Figs. 4b, 5 and 6; Giglio et al., 2006; Reid et al., 2009). Additional inclusion of daytime observations due to orbital convergence will typically be somewhat earlier or later in the afternoon and may therefore lower the FRE estimation. In the persistent approach, missing nighttime observations may cause an overestimation and missing daytime observation an underestimation of daily FRE, resulting in erroneous regional day-to-day variations in FRE estimates in the tropics (Fig. 6). Following previous research, we found that due to the spatiotemporal variation of the fire diurnal cycle FRE was overestimated more for some land cover types than for others (Table 2; Freeborn et al., 2011). Land cover classes that typically showed longer fire durations (Fig. 2c) with peak fire activity later in the afternoon (Fig. 2d) were not as much overestimated as land cover classes with more pronounced fire diurnal cycles (Figs. 5 and 6; Table 2). However, part of this effect likely stems from these land covers mostly being located in the more frequently observed higher latitudes of our study region. Although the persistent method is not directly comparable to the methods of widely used emission inventories like GFAS or QFED (Kaiser et al., 2012; Darmenov and da Silva, 2013), they likely introduce similar errors by ignoring the fire diurnal cycle.

When using the dynamic approach (based on a Gaussian function optimally fitted to the FRP observations at MODIS detection opportunities; Sect. 3.5), a general underestimation of FRE was seen when compared to that derived from the full SEVIRI

ACPD
15, 9661–9707, 2015

time-series, mostly due to underestimation of small fires (compare Figs. 3c and 5b). When optimally fitting a Gaussian function to a single FRP detection, the function will only reproduce the peak within the hour, while ignoring that a single fire detection at MODIS detection opportunity often represents a fire event lasting for several hours. The climatological approach, based on the climatology of the fire diurnal cycle, had by far the best performance in terms of absolute FRE estimation. In contrast to the persistent approach, in the dynamic and climatological approaches the hourly predictions were based on the last 24 h of fire activity, enabling more realistic gap filling during periods without observations. This resulted in an advantage during periods of cloud cover or missing observations due to the satellite orbits, but because of the low number of actual daily observations these modelling approaches had the tendency to continue predicting fire activity after fires had ceased, seen as a small delay in the signals in Fig. 6.

An additional criterion to evaluate the model performance was the correlation between the three modelling approaches and the SEVIRI data at different spatiotemporal scales. At 0.1° spatial and daily temporal resolution the persistent approach performed best, likely because it only predicts fire activity on days of actual fires while the other two methods may predict fire activity with some delay. Because of the large day-to-day variation in the diurnal cycle and the FRP measurements at the time of the MODIS overpasses, the individual FRP observations have a low precision (i.e., large random error) and omission (i.e., non detection) of fires is frequent (Figs. 1 and 4), resulting in low correlation at high spatiotemporal scales (Tables 3 and 4). Since fires rarely occur on their own and generally form part of a regional pattern (Bella et al., 2006), the correlation increased considerably when accumulating results to a 1° spatial scale, and at this scale the persistent and climatological approaches performed equally well (Table 3). For the same reason model performance was found to be best in savannas and woody savannas, where the highest number of fires occur and the sample size is thus largest, or in areas of large fire size where omission was relatively low.

ACPD
15, 9661–9707, 2015

Correlation at an hourly resolution was lower than at daily resolution, but a similar increase in model performance was found when aggregating to coarser spatial scales. Because often only a reasonably large sample of observations made at the MODIS detection opportunities is actually representative of fire activity in a certain region, the added value of the 0.1° spatial resolution (e.g., GFASv1.1/1.2) is somewhat limited compared to a coarser 0.5° spatial resolution (e.g., GFASv1.0). As could be expected, the dynamic and climatological approaches performed better at the hourly resolution, compared to the persistent approach that ignored fire diurnal cycle. Overall, using the climatological approach led to the best model performance, although in specific cases using the persistent or dynamic approach showed better results. The climatological approach used mean values for the fire duration σ and may therefore overestimate FRE from smaller fires while underestimating the larger fires.

Within GFAS, to handle the uncertainties introduced into the MODIS-derived FRE estimates by neglecting the diurnal cycle influence, the estimated FRE is converted into estimates of dry matter burned (DM) using land cover-specific conversion factors. These were derived via comparison of long-term monthly FRE estimates to the DM estimates calculated over the same period by the Global Fire Emissions Database (GFED 3.1; van der Werf et al., 2010; Kaiser et al., 2012). It is currently assumed that by allowing the conversion factors to vary with land cover type the impact of any land cover-varying diurnal cycle is also incorporated, reducing the influence of the diurnal cycle. The issues discussed above, along with the accuracy of the GFED DM calculations, which are for example affected by the quality of the burned area product and the biochemical models used, all influence values of the land cover-specific FRE-to-DM conversions factors presented by Kaiser et al. (2012).

Wooster et al. (2005) and Freeborn et al. (2008) previously explored the conversion factors between FRE and DM using small scale experiments, and found that they appeared relatively independent of vegetation type. However, when moving to the satellite-scale there are additional factors influencing this FRE-to-DM relationship, for example the fire regime of an area and the degree to which MODIS misses the

ACPD
15, 9661–9707, 2015

lowest FRP fires, and the canopy density of trees that might obscure some of the thermal radiation being emitted by fires burning in the ground fuels (Freeborn et al., 2014). The thermal radiation recorded in satellite products is additionally reduced by cloud cover and erroneous flagging of smoke as clouds during data processing. Konovalov et al. (2014) nevertheless found FRE-to-DM relationships relatively similar to those of the earlier small-scale experiments when using atmospheric observations and biomass burning trace gas and aerosol emissions factors to estimate fuel consumption. Exploring methods to incorporate the fire diurnal cycle in the GFAS global FRP-based near real time emission inventory is a first step in taking into account some of these issues in order to improve global FRE estimates made at relatively high spatiotemporal resolutions, and hopefully also in reconciling some of the differences in current emission inventories.

6 Conclusions

Emission inventories based on FRP observations have great potential to improve biomass burning emission estimates, by eliminating the need for modelling of fuel loads and fuel consumption, and can be produced in near real time. However, to date uncertainties in FRE estimation remain high when using polar orbiting FRP datasets, largely due to difficulties in combining the limited temporal resolution observations and knowledge about the fire diurnal cycle. Geostationary data can alleviate this issue, but brings its own problems related to the non-detection of the lower FRP fires due to the coarse spatial resolution of the geostationary observations. Geostationary dataset are also not global in extent. Here we explored the spatial dependencies of the fire diurnal cycle and its impact on active fire detections made at the time of MODIS overpasses. Three methods were developed to derive hourly FRE estimates based on data-assimilation and SEVIRI FRP observations subsampled at MODIS detection opportunities, and we evaluated these against the actual hourly FRP observations made by SEVIRI. Our main conclusions are:

ACPD
15, 9661–9707, 2015

1. We considered various drivers of the spatial distribution of fire diurnal cycle: dominant land cover, fire size, annual number of fire days, and diurnal climate conditions and found that all played a role. The strong relation between fire size and fire diurnal cycle for grass fuelled fires, and the climatic gradient in diurnal cycle, indicate that using fuel characteristics rather than land cover alone to characterize the fire diurnal cycle provides a potential pathway to improve these estimates. Here we showed that this information can partly be obtained by studying the fire characteristics, such as fire size, which are contained within the remote sensing data themselves.

2. Ignoring the fire diurnal cycle may cause structural errors in FRE estimates, and likely results in a general overestimation of FRE due to the timing of the MODIS overpasses. The errors vary regionally, mostly due to variations in the fire diurnal cycle, while results get more accurate at higher latitudes due to the increasing number of daily MODIS detection opportunities caused by orbital convergence.

3. Due to the large day-to-day variations in the fire diurnal cycle at the grid cell level, and the scarce number of MODIS observations of any one location per day, daily FRP fields calculated from observations made at MODIS detection opportunities are characterized by low precision (i.e., observations are not representative for daily fire activity) and high omission (i.e., non observation of fires). Therefore a sufficiently large sample size of MODIS observations is required to accurately estimate FRE, as shown earlier by Freeborn et al. (2011). In zones of frequent fires, where fires are generally part of a regional biomass burning pattern, model performance greatly improved when moving to a coarser scale, increasing the sample size. Model performance was also considerably better for zones of relatively large fires that were characterized by low omission. Production of emission inventories at very high spatiotemporal resolution using data from a limited number of low-Earth orbit satellite observations may therefore provide somewhat restricted added value compared to those derived at coarser spatiotemporal scales.

ACPD
15, 9661–9707, 2015

4. Relative overrepresentation of day- or nighttime FRP observations may cause large day to day variations in estimated FRE when the diurnal cycle is ignored.

5. The way we observe the fire diurnal cycle is scale dependent, mostly because of the large variation in fire diurnal cycle, even within the same grid cell between different days.

We recommend implementing the climatological model within GFAS in Copernicus Atmosphere Services in order to improve global and regional FRE estimates and further reconcile emission estimates from the various different inventories currently available.

Acknowledgements. We like to thank Samuel Remy at ECMWF for processing MODIS and SEVIRI data, and the data providing agencies: NASA and the EUMETSAT LSA SAF for making their data publicly available. This study was funded by the EU in the FP7 and H2020 projects MACC-II and MACC-III (contracts no. 283 576 and 633 080).

References

Archibald, S. and Roy, D. P.: Identifying individual fires from satellite-derived burned area data, IEEE Int. Geosci. Remote Sens. Symp. Proc., 9, 160–163, doi:10.1109/IGARSS.2009.5417974, 2009.

Archibald, S., Lehmann, C. E. R., Gómez-Dans, J. L., and Bradstock, R. A.: Defining pyromes and global syndromes of fire regimes, P. Natl. Acad. Sci. USA, 110, 6442–6447, doi:10.1073/pnas.1211466110, 2013.

Baldassarre, G., Pozzoli, L., Schmidt, C. C., Unal, A., Kindap, T., Menzel, W. P., Whitburn, S., Coheur, P.-F., Kavgaci, A., and Kaiser, J. W.: Using SEVIRI fire observations to drive smoke plumes in the CMAQ air quality model: the case of Antalya in 2008, Atmos. Chem. Phys. Discuss., 15, 1–46, doi:10.5194/acpd-15-1-2015, 2015.

Bella, C. M., Jobbagy, E. G., Paruelo, J. M., and Pinnock, S.: Continental fire density patterns in South America, Global Ecol. Biogeogr., 15, 192–199, doi:10.1111/j.1466-822X.2006.00225.x, 2006.

ACPD
15, 9661–9707, 2015

Boschetti, L. and Roy, D. P.: Strategies for the fusion of satellite fire radiative power with burned area data for fire radiative energy derivation, J. Geophys. Res., 114, D20302, doi:10.1029/2008JD011645, 2009.

Bowman, D. M. J. S., Balch, J. K., Artaxo, P., Bond, W. J., Carlson, J. M., Cochrane, M. A., D'Antonio, C. M., Defries, R. S., Doyle, J. C., Harrison, S. P., Johnston, F. H., Keeley, J. E., Krawchuk, M. A., Kull, C. A., Marston, J. B., Moritz, M. A., Prentice, I. C., Roos, C. I., Scott, A. C., Swetnam, T. W., van der Werf, G. R., and Pyne, S. J.: Fire in the Earth system, Science, 324, 481–484, doi:10.1126/science.1163886, 2009.

Darmenov, A. S. and da Silva, A.: The Quick Fire Emissions Dataset (QFED) – Documentation of Versions 2.1, 2.2 and 2.4, NASA Tech. Rep. Ser. Glob. Model. Data Assim., Greenbelt, USA, 32, 2013.

Ellicott, E., Vermote, E., Giglio, L., and Roberts, G.: Estimating biomass consumed from fire using MODIS FRE, Geophys. Res. Lett., 36, L13401, doi:10.1029/2009GL038581, 2009.

Freeborn, P. H., Wooster, M. J., Hao, W. M., Ryan, C. A., Nordgren, B. L., Baker, S. P., and Ichoku, C.: Relationships between energy release, fuel mass loss, and trace gas and aerosol emissions during laboratory biomass fires, J. Geophys. Res., 113, D01301, doi:10.1029/2007JD008679, 2008.

Freeborn, P. H., Wooster, M. J., Roberts, G., Malamud, B. D., and Xu, W.: Development of a virtual active fire product for Africa through a synthesis of geostationary and polar orbiting satellite data, Remote Sens. Environ., 113, 1700–1711, doi:10.1016/j.rse.2009.03.013, 2009.

Freeborn, P. H., Wooster, M. J., and Roberts, G.: Addressing the spatiotemporal sampling design of MODIS to provide estimates of the fire radiative energy emitted from Africa, Remote Sens. Environ., 115, 475–489, doi:10.1016/j.rse.2010.09.017, 2011.

Freeborn, P. H., Wooster, M. J., Roberts, G., and Xu, W.: Evaluating the SEVIRI fire thermal anomaly detection algorithm across the Central African Republic using the MODIS active fire product, Remote Sens. Environ., 6, 1890–1917, doi:10.3390/rs6031890, 2014.

Freitas, S. R., Longo, K. M., Silva Dias, M. A. F., Silva Dias, P. L., Chatfield, R., Prins, E., Artaxo, P., Grell, G. A., and Recuero, F. S.: Monitoring the transport of biomass burning emissions in South America, Environ. Fluid Mech., 5, 135–167, doi:10.1007/s10652-005-0243-7, 2005.

Friedl, M. A., McIver, D. K., Hodges, J. C. F., Zhang, X. Y., Muchoney, D., Strahler, A. H., Woodcock, C. E., Gopal, S., Schneider, A., Cooper, A., Baccini, A., Gao, F., and Schaaf, C.: Global

ACPD
15, 9661–9707, 2015

land cover mapping from MODIS: algorithms and early results, Remote Sens. Environ., 83, 287–302, doi:10.1016/S0034-4257(02)00078-0, 2002.
Gambiza, J., Campbell, B. M., Moe, S. R., and Frost, P. G. H.: Fire behaviour in a semi-arid Baikiaea plurijuga savanna woodland on Kalahari sands in western Zimbabwe, S. Afr. J. Sci., 101, 239–244, 2005.
Giglio, L.: Characterization of the tropical diurnal fire cycle using VIRS and MODIS observations, Remote Sens. Environ., 108, 407–421, doi:10.1016/j.rse.2006.11.018, 2007.
Giglio, L., Justice, C. O., and Csiszar, I.: Global distribution and seasonality of active fires as observed with the Terra and Aqua Moderate Resolution Imaging Spectroradiometer (MODIS) sensors, J. Geophys. Res., 111, G02016, doi:10.1029/2005JG000142, 2006.
Giglio, L., Loboda, T., Roy, D. P., Quayle, B., and Justice, C. O.: An active-fire based burned area mapping algorithm for the MODIS sensor, Remote Sens. Environ., 113, 408–420, doi:10.1016/j.rse.2008.10.006, 2009.
Giglio, L., Randerson, J. T., and van der Werf, G. R.: Analysis of daily, monthly, and annual burned area using the fourth-generation global fire emissions database (GFED4), J. Geophys. Res.-Biogeo., 118, 317–328, doi:10.1002/jgrg.20042, 2013.
Hély, C., Alleaume, S., Swap, R. J., Shugart, H. H., and Justice, C. O.: SAFARI-2000 characterization of fuels, fire behavior, combustion completeness, and emissions from experimental burns in infertile grass savannas in western Zambia, J. Arid Environ., 54, 381–394, doi:10.1006/jare.2002.1097, 2003.
Ichoku, C., Giglio, L., Wooster, M. J., and Remer, L. A.: Global characterization of biomass-burning patterns using satellite measurements of fire radiative energy, Remote Sens. Environ., 112, 2950–2962, doi:10.1016/j.rse.2008.02.009, 2008.
Johnston, F. H., Henderson, S. B., Chen, Y., Randerson, J. T., Marlier, M., Defries, R. S., Kinney, P., Bowman, D. M. J. S., and Brauer, M.: Estimated global mortality attributable to smoke from landscape fires, Environ. Health Persp., 120, 695–701, doi:10.1289/ehp.1104422, 2012.
Kaiser, J. W., Flemming, J., Schultz, M. G., Suttie, M., and Wooster, M. J.: The MACC Global Fire Assimilation System: First Emission Products (GFASv0), Tech. Memo. 596, ECMWF, Reading, UK, 2009.
Kaiser, J. W., Heil, A., Andreae, M. O., Benedetti, A., Chubarova, N., Jones, L., Morcrette, J.-J., Razinger, M., Schultz, M. G., Suttie, M., and van der Werf, G. R.: Biomass burning emissions

ACPD
15, 9661–9707, 2015

estimated with a global fire assimilation system based on observed fire radiative power, Biogeosciences, 9, 527–554, doi:10.5194/bg-9-527-2012, 2012.
Konovalov, I. B., Berezin, E. V., Ciais, P., Broquet, G., Beekmann, M., Hadji-Lazaro, J., Clerbaux, C., Andreae, M. O., Kaiser, J. W., and Schulze, E.-D.: Constraining CO_2 emissions from open biomass burning by satellite observations of co-emitted species: a method and its application to wildfires in Siberia, Atmos. Chem. Phys., 14, 10383–10410, doi:10.5194/acp-14-10383-2014, 2014.
Langmann, B., Duncan, B., Textor, C., Trentmann, J., and van der Werf, G. R.: Vegetation fire emissions and their impact on air pollution and climate, Atmos. Environ., 43, 107–116, doi:10.1016/j.atmosenv.2008.09.047, 2009.
Larkin, N. K., Raffuse, S. M., and Strand, T. M.: Wildland fire emissions, carbon, and climate: US emissions inventories, Forest Ecol. Manag., 317, 61–69, doi:10.1016/j.foreco.2013.09.012, 2014.
Mu, M., Randerson, J. T., van der Werf, G. R., Giglio, L., Kasibhatla, P., Morton, D. C., Collatz, G. J., DeFries, R. S., Hyer, E. J., Prins, E. M., Griffith, D. W. T., Wunch, D., Toon, G. C., Sherlock, V., and Wennberg, P. O.: Daily and 3 hourly variability in global fire emissions and consequences for atmospheric model predictions of carbon monoxide, J. Geophys. Res.-Atmos., 116, D24303, doi:10.1029/2011JD016245, 2011.
Prins, E. M. and Menzel, W. P.: Geostationary satellite detection of biomass burning in South America, Int. J. Remote Sens., 13, 2783–2799, doi:10.1080/01431169208904081, 1992.
Randerson, J. T., Chen, Y., van der Werf, G. R., Rogers, B. M., and Morton, D. C.: Global burned area and biomass burning emissions from small fires, J. Geophys. Res., 117, G04012, doi:10.1029/2012JG002128, 2012.
Reid, J. S., Hyer, E. J., Prins, E. M., Westphal, D. L., Zhang, J., Wang, J., Christopher, S. A., Curtis, C. A., Schmidt, C. C., Eleuterio, D. P., Richardson, K. A., and Hoffman, J. P.: Global monitoring and forecasting of biomass-burning smoke: description of and lessons from the Fire Locating and Modeling of Burning Emissions (FLAMBE) program, IEEE J. Sel. Top. Appl., 2, 144–162, doi:10.1109/JSTARS.2009.2027443, 2009.
Roberts, G. J. and Wooster, M. J.: Fire detection and fire characterization over Africa using meteosat SEVIRI, IEEE T. Geosci. Remote, 46, 1200–1218, doi:10.1109/TGRS.2008.915751, 2008.
Roberts, G., Wooster, M. J., Perry, G. L. W., Drake, N., Rebelo, L.-M., and Dipotso, F.: Retrieval of biomass combustion rates and totals from fire radiative power observations: application

ACPD
15, 9661–9707, 2015

to southern Africa using geostationary SEVIRI imagery, J. Geophys. Res., 110, D21111, doi:10.1029/2005JD006018, 2005.
Roberts, G., Wooster, M. J., and Lagoudakis, E.: Annual and diurnal african biomass burning temporal dynamics, Biogeosciences, 6, 849–866, doi:10.5194/bg-6-849-2009, 2009.
Roberts, G., Wooster, M. J., Freeborn, P. H., and Xu, W.: Integration of geostationary FRP and polar-orbiter burned area datasets for an enhanced biomass burning inventory, Remote Sens. Environ., 115, 2047–2061, doi:10.1016/j.rse.2011.04.006, 2011.
Roy, D. P., Jin, Y., Lewis, P. E., and Justice, C. O.: Prototyping a global algorithm for systematic fire-affected area mapping using MODIS time series data, Remote Sens. Environ., 97, 137–162, doi:10.1016/j.rse.2005.04.007, 2005.
Schmetz, J., Pili, P., Tjemkes, S., Just, D., Kerkmann, J., Rota, S., and Ratier, A.: An introduction to Meteosat Second Generation (MSG), B. Am. Meteorol. Soc., 83, 977–991, doi:10.1175/BAMS-83-7-Schmetz-1, 2002.
Seiler, W., and Crutzen, P. J.: Estimates of gross and net fluxes of carbon between the biosphere and the atmosphere from biomass burning, Climatic Change, 2, 207–247, doi:10.1007/BF00137988, 1980.
Sofiev, M., Vankevich, R., Lotjonen, M., Prank, M., Petukhov, V., Ermakova, T., Koskinen, J., and Kukkonen, J.: An operational system for the assimilation of the satellite information on wild-land fires for the needs of air quality modelling and forecasting, Atmos. Chem. Phys., 9, 6833–6847, doi:10.5194/acp-9-6833-2009, 2009.
Sofiev, M., Vankevich, R., Ermakova, T., and Hakkarainen, J.: Global mapping of maximum emission heights and resulting vertical profiles of wildfire emissions, Atmos. Chem. Phys., 13, 7039–7052, doi:10.5194/acp-13-7039-2013, 2013.
Sow, M., Hély, C., Mbow, C., and Sambou, B.: Fuel and fire behavior analysis for early-season prescribed fire planning in Sudanian and Sahelian savannas, J. Arid Environ., 89, 84–93, doi:10.1016/j.jaridenv.2012.09.007, 2013.
van der Werf, G. R., Randerson, J. T., Giglio, L., Collatz, G. J., Mu, M., Kasibhatla, P. S., Morton, D. C., DeFries, R. S., Jin, Y., and van Leeuwen, T. T.: Global fire emissions and the contribution of deforestation, savanna, forest, agricultural, and peat fires (1997–2009), Atmos. Chem. Phys., 10, 11707–11735, doi:10.5194/acp-10-11707-2010, 2010.
Vermote, E., Ellicott, E., Dubovik, O., Lapyonok, T., Chin, M., Giglio, L., and Roberts, G. J.: An approach to estimate global biomass burning emissions of organic and black carbon from

ACPD
15, 9661–9707, 2015

MODIS fire radiative power, J. Geophys. Res., 114, D18205, doi:10.1029/2008JD011188, 2009.

Wiedinmyer, C., Akagi, S. K., Yokelson, R. J., Emmons, L. K., Al-Saadi, J. A., Orlando, J. J., and Soja, A. J.: The Fire INventory from NCAR (FINN): a high resolution global model to estimate the emissions from open burning, Geosci. Model Dev., 4, 625–641, doi:10.5194/gmd-4-625-2011, 2011.

Wooster, M. J., Roberts, G., Perry, G. L. W., and Kaufman, Y. J.: Retrieval of biomass combustion rates and totals from fire radiative power observations: FRP derivation and calibration relationships between biomass consumption, J. Geophys. Res., 110, D24311, doi:10.1029/2005JD006318, 2005.

Wooster, M. J., Roberts, G. J., Freeborn, P. H., Xu, W., Govaerts, Y., Beedy, R., He, J., and Mullen, R.: Meteosat SEVIRI Fire Radiative Power (FRP) products from the Land Surface Analysis Satellite Applications Facility (LSA SAF): Part 1 – algorithms, product contents and analysis, Atmos. Chem. Phys. Discuss., accepted, 2015.

Xu, W., Wooster, M. J., Roberts, G., and Freeborn, P.: New GOES imager algorithms for cloud and active fire detection and fire radiative power assessment across North, South and Central America, Remote Sens. Environ., 114, 1876–1895, doi:10.1016/j.rse.2010.03.012, 2010.

Zhang, X., Kondragunta, S., Ram, J., Schmidt, C., and Huang, H.-C.: Near-real-time global biomass burning emissions product from geostationary satellite constellation, J. Geophys. Res., 117, D14201, doi:10.1029/2012JD017459, 2012.

ACPD
15, 9661–9707, 2015

Table 1. Mean values of the parameters of the Gaussian function per land cover type (excluding days of cloud cover and weighted by FRE). Values of σ and the ratio of ρ_{peak} and mean daytime FRP at MODIS detection opportunities ($MODIS_{mean}$) were used within the climatological approach to model hourly FRP (see Sect. 3.6).

Land cover	σ (hour)	ρ_{peak} (MW)	ρ_{base} (MW)	h_{peak} (hour)	$\rho_{peak}/MODIS_{mean}$ (–)
Temporal forest	1.14	846	24.2	13.31	3.17
Tropical forest	0.85	1364	27.3	13.34	3.03
Woody savanna	0.94	1501	21.1	13.21	3.07
Savanna	1.09	1710	39.0	13.08	2.88
Shrubland	1.35	3079	108.9	13.16	2.87
Grassland	1.06	1642	37.3	12.95	3.08
Cropland	0.95	1259	23.9	13.33	2.94

ACPD
15, 9661–9707, 2015

Table 2. Estimated annual FRE during 2010–2012 by the three model approaches as percentage of SEVIRI FRE (cloud corrected).

Land cover	SEVIRI ($PJ\,yr^{-1}$)	Persistent (%)	Dynamic (%)	Climatological (%)
Temperate forest	2.9	98	53	118
Tropical forest	61.3	179	60	98
Woody savanna	1513.2	174	70	93
Savanna	990.7	155	77	99
Shrubland	91.7	120	73	115
Grassland	106.5	125	62	108
Cropland	74.5	147	63	90
Total	2841.9	163	72	97

ACPD
15, 9661–9707, 2015

Table 3. Pearson's r between daily FRE as observed by SEVIRI (cloud cover corrected) and estimated by the three modelling approaches. Correlation is calculated for two spatial scales, the original 0.1° resolution and a 1° aggregated resolution (in parentheses) to test regional model performance.

Land cover	Persistent	Dynamic	Climatological
Temperate forest	0.44 (0.50)	0.20 (0.40)	0.21 (0.39)
Tropical forest	0.32 (0.41)	0.13 (0.40)	0.16 (0.41)
Woody savanna	0.48 (0.80)	0.22 (0.78)	0.25 (0.79)
Savanna	0.54 (0.78)	0.25 (0.75)	0.30 (0.76)
Shrubland	0.61 (0.63)	0.30 (0.58)	0.37 (0.60)
Grassland	0.46 (0.55)	0.18 (0.51)	0.22 (0.52)
Cropland	0.42 (0.61)	0.13 (0.58)	0.18 (0.60)
Total	0.50 (0.76)	0.23 (0.74)	0.27 (0.75)

ACPD
15, 9661–9707, 2015

Table 4. Pearson's *r* between hourly FRE as observed by SEVIRI and estimated by the models for cloud free days. Correlation is calculated for two spatial scales, the original 0.1° resolution and a 1° aggregated resolution between brackets to test regional model performance.

Land cover	Persistent	Dynamic	Climatological
Temperate forest	0.24 (0.33)	0.19 (0.31)	0.20 (0.32)
Tropical forest	0.13 (0.25)	0.16 (0.27)	0.15 (0.27)
Woody savanna	0.19 (0.44)	0.20 (0.50)	0.20 (0.52)
Savanna	0.25 (0.45)	0.23 (0.48)	0.25 (0.51)
Shrubland	0.35 (0.47)	0.29 (0.46)	0.32 (0.47)
Grassland	0.22 (0.32)	0.19 (0.34)	0.20 (0.35)
Cropland	0.19 (0.32)	0.17 (0.35)	0.17 (0.36)
Total	0.22 (0.43)	0.21 (0.47)	0.22 (0.50)

ACPD
15, 9661–9707, 2015

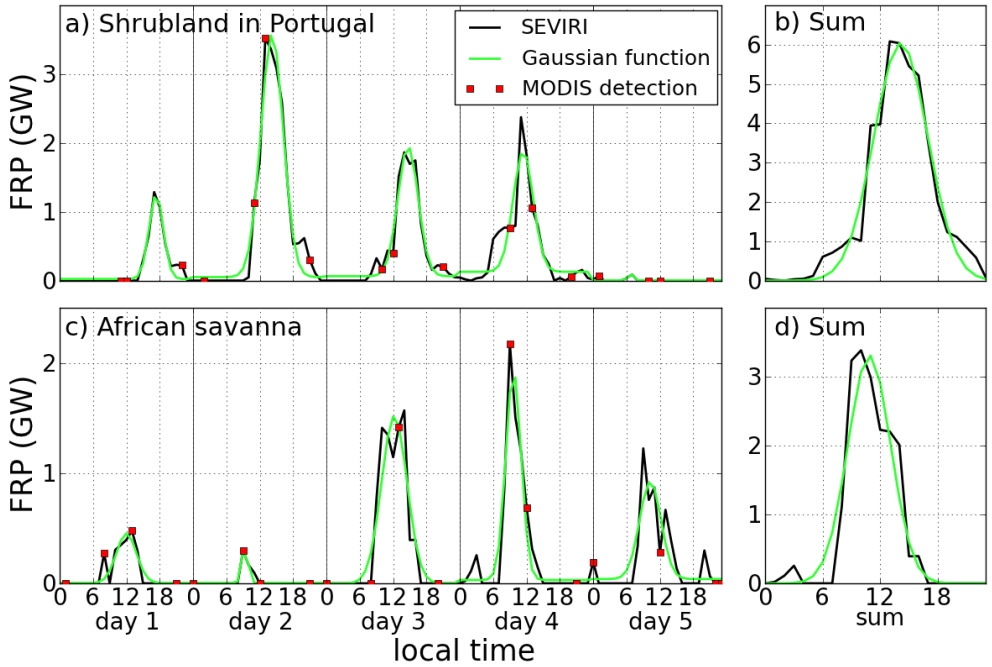

Figure 1. Hourly-mean FRP time-series derived from SEVIRI data, the same data but only sampled at MODIS detection opportunities, and an optimally fitted Gaussian function fitted to the full SEVIRI FRP time-series. These two examples are for a 0.1° shrubland grid cell in Portugal **(a, b)** and a 0.1° savanna grid cell in Africa **(c, d)**. **(a, c)** represent the hourly time-series and **(b, d)** the aggregated fire diurnal cycle over the 5 study days. Time is indicated as local time.

ACPD
15, 9661–9707, 2015

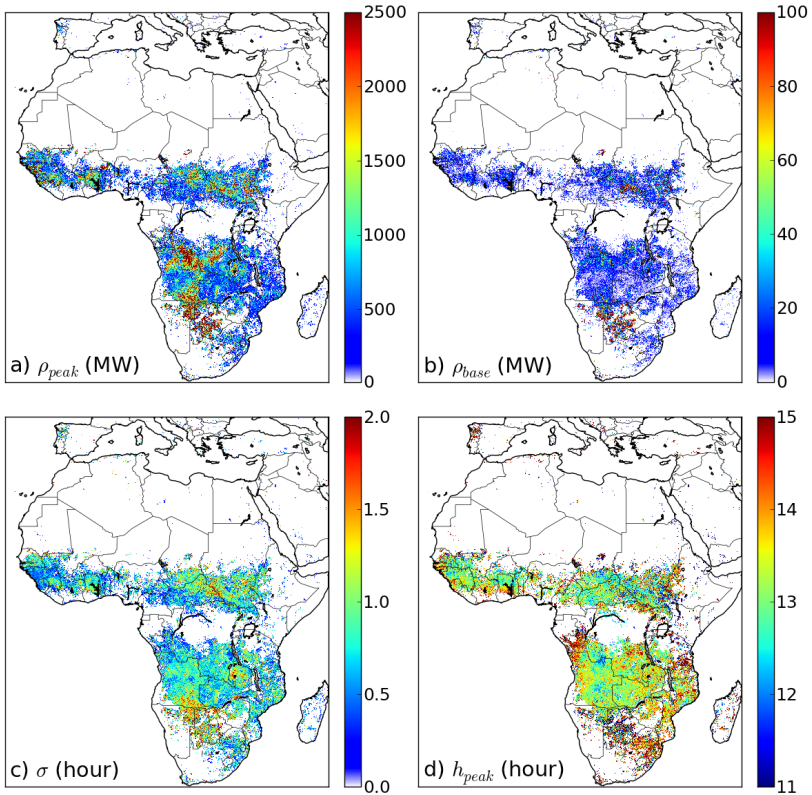

Figure 2. Weighted mean values of parameters of the optimally fitted Gaussian model for each 0.1° grid cell, including all cloud free days during the study period. **(a)** Peak daytime FRP ρ_{peak}, **(b)** night time FRP ρ_{base}, **(c)** SD of the FRE distribution over the day σ (related to the fire duration over the day, or width of the diurnal cycle), and **(d)** hour of peak fire activity h_{peak} (local time). Grid cells with emitted energy below 5 MJ over the study period (approximately the FRE emitted during one small fire event) were excluded from the figure to facilitate interpretation.

ACPD
15, 9661–9707, 2015

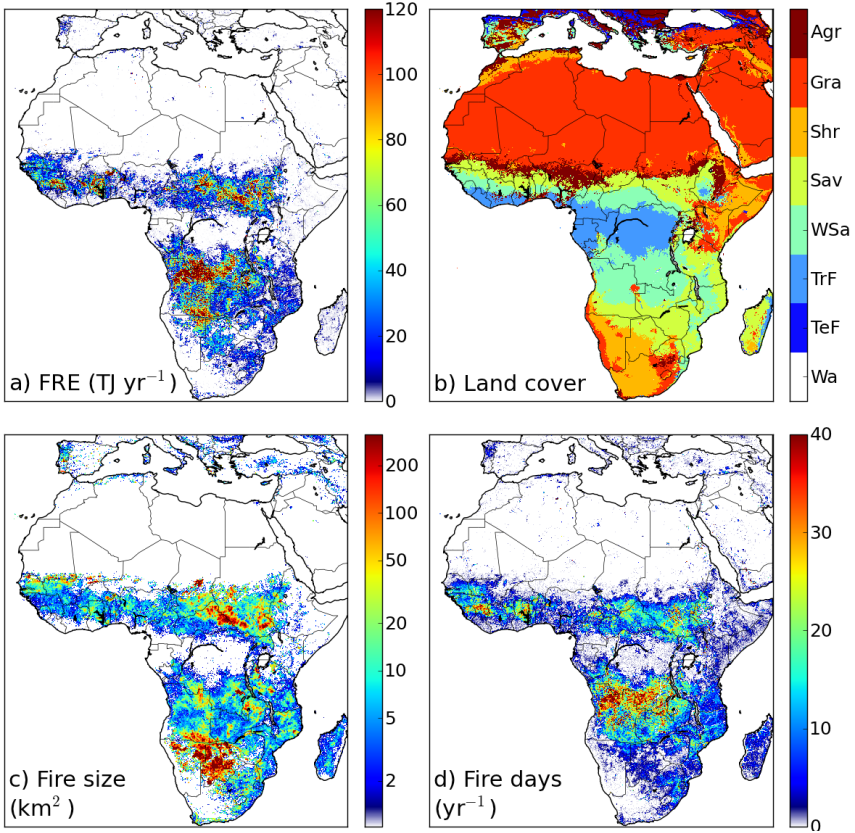

Figure 3. Characteristics of the fire regime and fuel types. **(a)** Mean annual FRE per 0.1° grid cell over the study period (2010–2012), **(b)** dominant land cover type, **(c)** fire size (2001–2013; i.e., weighted mean burned area per fire event) and **(d)** mean annual number of days with fire activity per grid cell over the study period. Abbreviations of land cover classes: water (Wa), temperate forest (TeF), tropical forest (TrF), woody savanna (WSa), savanna (Sav), shrubland (Shr), grassland (Gra) and agriculture (Agr).

ACPD
15, 9661–9707, 2015

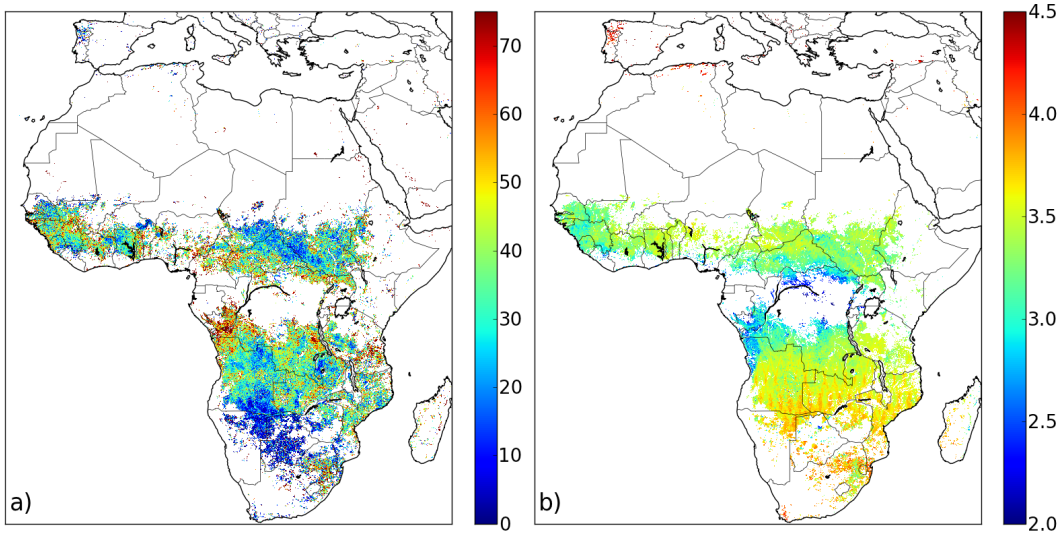

Figure 4. Detection of fire activity at MODIS detection opportunities. **(a)** Percentage of FRE emitted on days that the SEVIRI instrument did not observe active fires at MODIS overpasses. **(b)** Number of MODIS detection opportunities per day during the burning season (mean over the study period, weighted for monthly FRP).

ACPD
15, 9661–9707, 2015

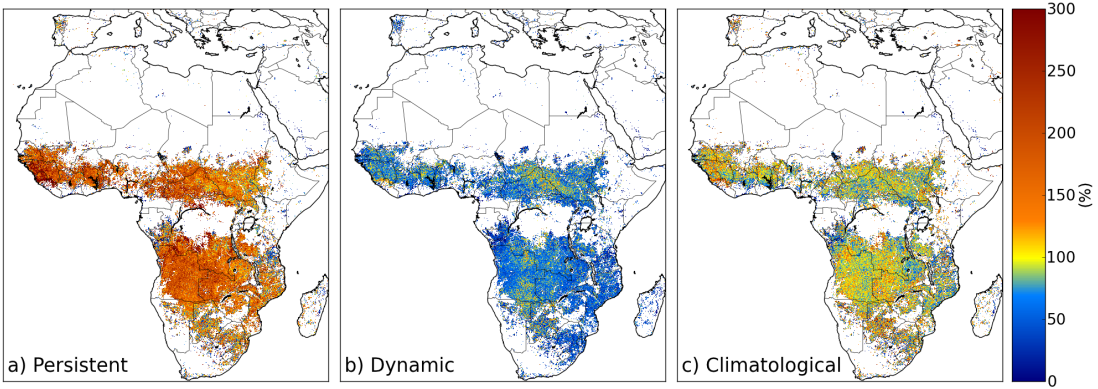

Figure 5. Total fire radiative energy (FRE) estimated via the three modelling approaches using SEVIRI observations taken at only the MODIS detection opportunities, expressed as fraction of the total FRE calculated using the entire set of hourly mean, 0.1° SEVIRI FRP observations (cloud cover corrected). **(a)** Persistent approach, **(b)** dynamic approach and **(c)** climatological approach.

ACPD
15, 9661–9707, 2015

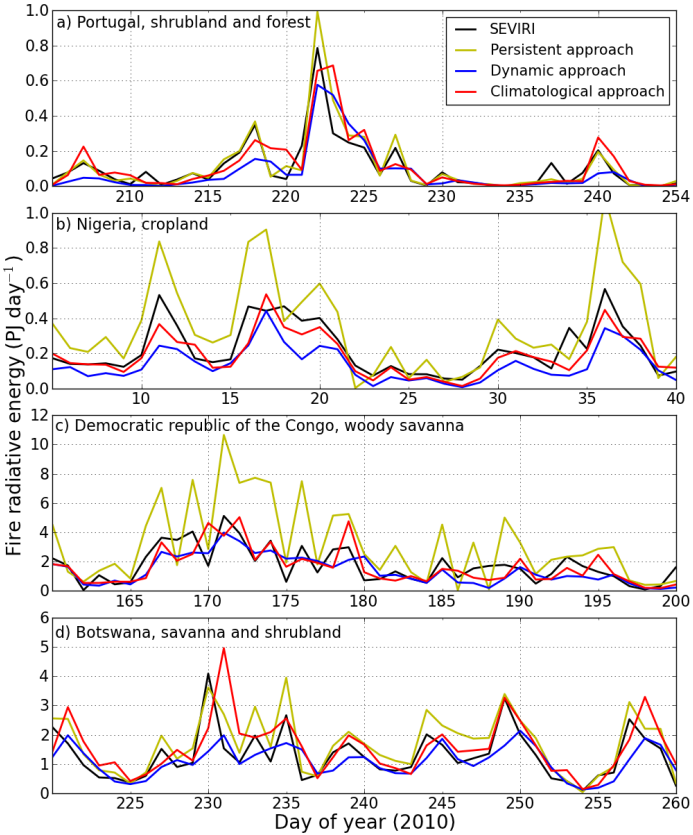

Figure 6. Daily FRE for three study regions (areas of 85 000 to 567 000 km^2) derived from the complete SEVIRI dataset (cloud cover corrected) and estimated by the three modelling approaches developed here. **(a)** Daily FRE for Portugal, mostly including shrublands and temperate forests, **(b)** fires in Nigeria burning in croplands, **(c)** woody savannas in DRC, and **(d)** shrublands and savannas in Botswana. Study regions are shown in Fig. 7, and land cover was determined using the dominant land cover classes (Sect. 2.3; Fig. 3b).

ACPD
15, 9661–9707, 2015

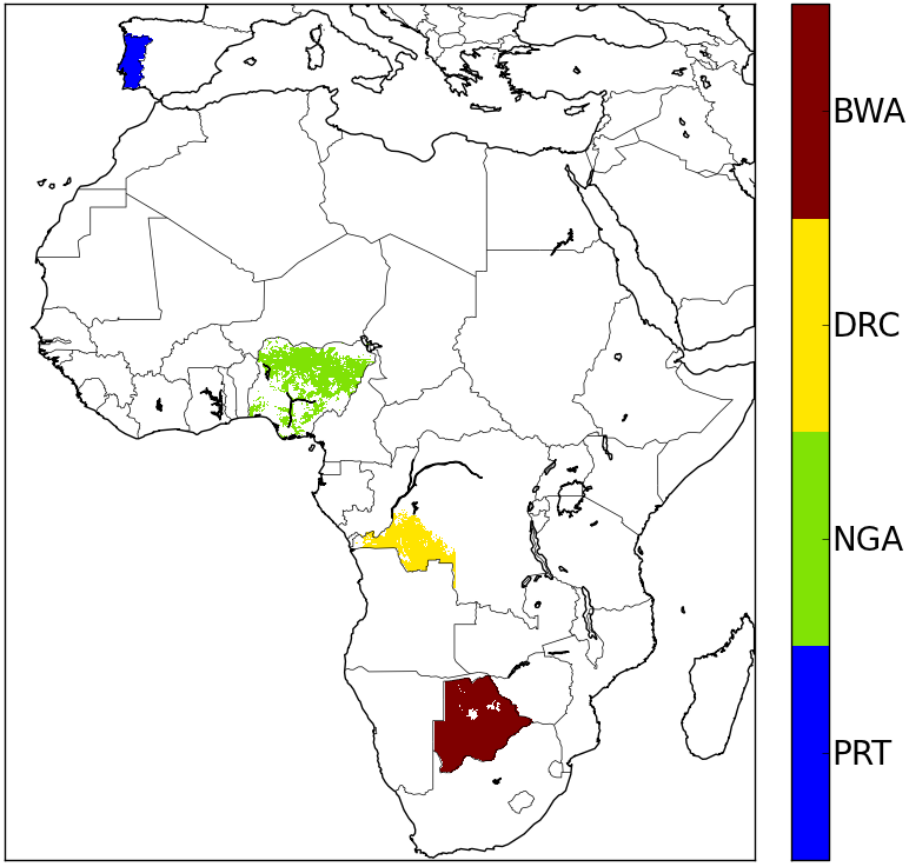

Figure 7. Study regions used in Fig. 6. Abbreviations refer to: Botswana (BWA), the Democratic Republic of the Congo (DRC), Nigeria (NGA) and Portugal (PRT).

ACPD
15, 9661–9707, 2015